Recibido: 13/03/2023
Aceptado: 07/07/2023

REVISTA DE TELEDETECCIÓN
Asociación Española de Teledetección
(2023) 62, 21-38
ISSN 1133-0953
EISSN 1988-8740
https://doi.org/10.4995/raet.2023.19368

Calibration of volumetric soil moisture using Landsat-8 and Sentinel-2 satellite imagery by Google Earth Engine

José Rodolfo Quintana-Molina[1*], Ignacio Sánchez-Cohen[2], Sergio Iván Jiménez-Jiménez[2], Mariana de Jesús Marcial-Pablo[2], Ricardo Trejo-Calzada[1], Emilio Quintana-Molina[3]

[1]*Natural Resources and Environment in Arid Zones Postgraduate. Chapingo Autonomous University-Regional University Unit of Arid Zones. Km. 40 Rd. Gómez Palacio Chihuahua Bermejillo, C.P. 35230, Durango, México.*

[2]*INIFAP-CENID RASPA National Center for Disciplinary Research on Water-Soil-Plant-Atmosphere Relationships, Right Sacramento Canal km 6.5, Industrial Zone, Gómez Palacio, CP. 35140, Durango, México.*

[3]*International Land and Water Management Program, Water Resources Management Chair Group, Wageningen University & Research, 6708 PB, Wageningen, Güeldres, Países Bajos.*

Abstract: Water scarcity for agriculture is increasingly evident due to climatic alterations and inadequate management of this resource. Therefore, developing digital models that help improve water resource management to provide solutions to agronomic problems in northern Mexico is necessary. In this context, the objective of the present research is to calibrate the Optical Trapezoidal (OPTRAM) and Thermal-Optical Trapezoidal (TOTRAM) models to estimate the volumetric soil moisture at different depths through vegetation indices derived from Landsat-8 and Sentinel-2 satellite images using Google Earth Engine (GEE). Agricultural areas under gravity irrigation and rainfed runoff in the Comarca Lagunera, the lower part of the Hydrological Region No. 36 of the Nazas and Aguanaval rivers were selected for in-situ measurements. The OPTRAM and TOTRAM normalized moisture content (W) estimates were compared with in-situ volumetric soil moisture (θ) data. Results indicate that the predictions of OPTRAM errors using Sentinel-2 images showed RMSE between 0.033 to 0.043 cm^3 cm^{-3} and R^2 between 0.66 to 0.75, whereas Landsat-8 errors showed RSME from 0.036 to 0.057 cm^3 cm^{-3} and R^2 between 0.70 to 0.81. On the other hand, TOTRAM errors showed RMSE between 0.045 to 0.053 cm^3 cm^{-3} and R^2 between 0.62 to 0.85 through calibrations. This study made it possible to evaluate the most accurate combinations of the pixel distributions of each model and vegetation indices for the estimation of volumetric soil moisture within the different phenological stages of the crops.

Key words: Satellite images, models, vegetation indices, pixel distributions.

Calibración de la humedad volumétrica del suelo utilizando imágenes Landsat-8 y Sentinel-2 mediante *Google Earth Engine*

Resumen: La escasez de agua para la agricultura es cada vez más evidente producto de las alteraciones climáticas y el inadecuado manejo de este recurso. Por ende, el desarrollo de modelos digitales que ayuden a la mejora del manejo de los recursos hídricos para proporcionar soluciones a los problemas agronómicos al norte de México es necesario. En este contexto, el objetivo de la presente investigación es calibrar los modelos Óptico Trapezoidal (OPTRAM) y Térmico-Óptico Trapezoidal (TOTRAM) para estimar la humedad volumétrica del suelo a diferentes profundidades a través de índices de vegetación derivados de imágenes de satelitales Landsat-8 y Sentinel-2 utilizando Google Earth Engine (GEE). Áreas agrícolas seleccionadas bajo riego por gravedad y temporal por

To cite this article: Quintana-Molina, J.R., Sánchez-Cohen, I., Jiménez-Jiménez, S.I., Marcial-Pablo, M.J., Trejo-Calzada, R., Quintana-Molina, E. 2023. Calibration of volumetric soil moisture using Landsat-8 and Sentinel-2 satellite imagery by Google Earth Engine. *Revista de Teledetección*, *62*, 21-38. https://doi.org/10.4995/raet.2023.19368

* *Corresponding author: rodolfoquintanam97@gmail.com*

escorrentías en la Comarca Lagunera, parte baja de la Región Hidrológica No. 36 de los ríos Nazas y Aguanaval fueron seleccionadas para mediciones in-situ. Las estimaciones del contenido normalizado de humedad (W) de OPTRAM y TOTRAM fueron comparados con datos de humedad volumétrica del suelo (θ) *in-situ*. Los resultados indican que las predicciones de los errores de OPTRAM utilizando imágenes Sentinel-2 mostraron RMSE entre 0,033 a 0,043 cm^3 cm^{-3} y R^2 entre 0,66 a 0,75. Mientras, los errores de Landsat-8 mostraron RSME de 0,036 a 0,057 cm^3 cm^{-3} y R^2 entre 0,70 a 0,81. Por otra parte, los errores de TOTRAM mostraron RMSE entre 0,045 a 0,053 cm^3 cm^{-3} y R^2 entre 0,62 a 0,85 a través de las calibraciones. Este estudio permitió evaluar, las combinaciones más precisas de las distribuciones de los píxeles de cada modelo e índice de vegetación para la estimación de humedad volumétrica del suelo dentro de las distintas etapas fenológicas de los cultivos.

Palabras clave: imágenes de satélite, modelos, índices de vegetación, distribución de los píxeles.

1. Introduction

Soil moisture is considered a fundamental variable in hydrological processes such as infiltration, runoff, and evaporation (Vereecken et al., 2008; Rahmati et al., 2018) and agronomic processes such as crop yield and efficiency (Tollenaar & Lee, 2002). Soil moisture is highly variable in time and space due to the heterogeneity of soil properties, topography, land cover, evapotranspiration, and precipitation uniformity (Santos et al., 2014). Field measurement of soil moisture is costly, time-consuming, and impractical for continuous temporal and spatial monitoring at different scales (Rahimzadeh-Bajgiran et al., 2013). Field sampling techniques such as Time Domain Reflectometry (TDR) and gravimetric can provide quantitatively accurate measurements of soil moisture, but with the disadvantage that they do not consider changes in spatial distributions across all soil surface features (Lakhankar et al., 2009). Studies as Dobriyal et al. (2012) give a review available for estimating soil moisture and criteria for direct (gravimetric, neutron probe, time dominian reflectometry, tensiometer, etc.) and indirect (gamma ray attenuation, retome sensing, capacitance sensor, gypsum block, pressure plate, etc.) methods such as cost effectiveness, accuracy, spatial scale, response time and measured parameter. This study will be helpful for researchers in any field to select the appropiate method keeping in view the time and resources available to them in order to improve the productivity and water managment. Therefore, remote sensing (RS) through various techniques uses the optical, thermal, and microwave regions of the electromagnetic spectrum developed to estimate soil surface moisture (Wang & Qu, 2009; Şekertekin et al., 2018). Microwave techniques have shown much greater potential in soil moisture monitoring, as microwaves can penetrate the vegetation canopy and cloud cover (Tabatabaeenejad et al., 2015). However, microwaves are unsuitable for small-scale applications due to their coarse resolution. On the other hand, the essential advantage of thermal and optical techniques over microwaves is that they provide a spatial resolution that can be used at small scales (Lakshmi, 2012). The Thermo-Optical Trapezoid Model (TOTRAM) developed by Moran et al. (1994) integrates the spectrum of vegetation indices (VI) with land surface temperature (LST) measurements. TOTRAM is applicable for crops entirely or partially covered by vegetation. More recently, different modifications to the traditional trapezoid model have been proposed (Mallick et al. 2009). Despite its success, the application of TOTRAM suffers from two limitations. The first limitation is that it requires satellite missions containing optical and thermal observations, while some satellites, such as Sentinel-2, do not provide thermal information. The second limitation is that LST requires individual parameterization for each observed date because LST depends not only on soil moisture but also on atmospheric environmental parameters such as near-surface air temperature, relative humidity, and wind speed (Pandey et al., 2021). Parameterization and calibration can be implemented agronomically for an entire crop season once prepared for a particular area. Because of the existing limitations, Sadeghi et al. (2017) proposed the Optical Trapezoid Model (OPTRAM), based on the linear relationship between soil moisture and reflectance transformed shortwave infrared (STR) in order to replace the LST of TOTRAM and can be implemented for soil moisture estimation using Sentinel-2 imagery. The OPTRAM model has been applied for agricultural

drought control, soil moisture estimation and moisture monitoring in irrigated and rainfed crops (Mananze et al., 2019; Ambrosone et al., 2020).

The present investigation includes a two-year time series combination analysis of the pixel distributions of the relationships between LST and STR in conjunction with NDVI, SAVI, and MSAVI vegetation indices of surface irrigation and rainfed agriculture to calibrate and validate the normalized moisture content (W) through the OPTRAM and TOTRAM optical models. The W data were compared with measured volumetric soil moisture data (Θ) at 5, 10, and 20 cm depths. These analyses made it possible to know the vegetation index (VI), model (OPTRAM/TOTRAM), and linear relationship (W-Θ) with the highest accuracy at different depths for estimating volumetric soil moisture.

2. Materials and methods

2.1. Study area

The study was performed in three agricultural areas of the Comarca Lagunera, the lower part of Hydrological Region No. 36, located in the southeast of the municipality of Mapimi, Durango, Mexico (Figure 1). Soil Texture Triangle developed by the USDA (U.S.D.A, 1977) and Bouyoucos method (Bouyoucos, 1936) were used for soil characterization using a composite soil sample for each area (Table 1). According to the Köppen classification modified by García (2004), Mapimi presents an arid and highly semi-warm climate with rainfall in summer. Precipitation occurs in violent downpours of short duration with an annual average of 264.2 mm with a maximum of 513 mm and a minimum of 81 mm. The yearly temperature is 20.8 °C with an average winter minimum of 3.9 °C and an average summer maximum of 36.1 °C (Montaña, 1988). The soils are characterized by low organic matter (OM), phosphorus (P), and calcium (Ca), high saline and sodium concentrations with soils types such as yermosol, xerosol, regosol and litosol (Ramírez and Pedroza, 2007), especially in the lower areas.

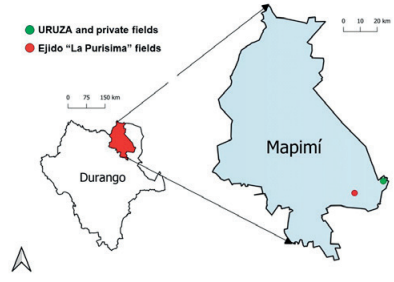

Figure 1. Location of the municipality of Mapimi, Durango, and agricultural areas (own elaboration).

2.2. Methods for calculating volumetric soil moisture in the field

The volumetric soil moisture data calculated by the gravimetric method (Dane & Topp, 2002) correspond to The Chapingo Autonomous University - URUZA fields (Figure 2a) and the

Table 1. Characteristics of agricultural areas.

Chapingo Autonomous University-Regional University Unit of Arid Zones (URUZA) fields	Private fields near the Regional University Unit of Arid Zones (URUZA)	Private agricultural fields in Ejido "La Purísima"
Coordinates 103° 35' 52" W longitude, 25° 53' 47" N latitude.	Coordinates 103° 36' 12" W longitude, 25° 53' 8" N latitude.	Coordinates 103° 46' 9" W longitude, 25° 49' 57" N latitude.
Self-consumption fodder sorghum crop (URUZA).	Growing forage sorghum for sale to dairies.	Monoculture of forage corn for self-consumption.
Texture type sandy loam at 0-30 cm and 30-60 cm depth.	Texture type sandy loam at 0-30 cm and 30-60 cm depth.	Texture type loam at 0-30 cm and 30-60 cm depth.
Surface irrigation agriculture with 7.21 ha, irrigation of one watering and four irrigations from October to February.	Surface irrigation agriculture with 9.05 ha, irrigation of one watering and four irrigations from March to August.	Rainfed agriculture with 1.62 ha, irrigation based on runoff from a hydrological basin from July to November.

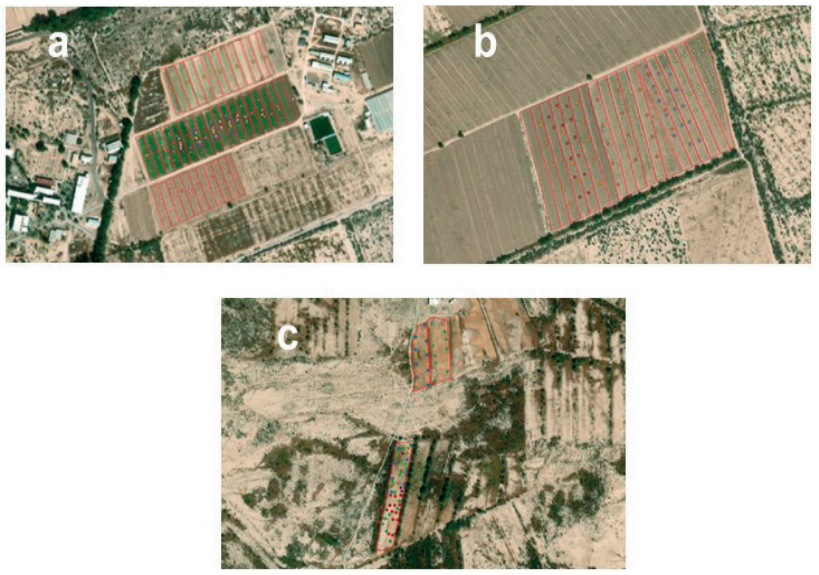

Figure 2. (a) Chapingo Autonomous University- Regional University Unit of Arid Zones (URUZA) fields, (b) private fields near the URUZA, (c) Ejido "La Purísima" private fields, images extracted from Google Earth Engine.

private fields near URUZA (Figure 2b). On the other hand, time domain reflectometry (TDR) method (Davis & Chudoviak, 1975) used a Decagon Devices ® ProCheck Version 4 and the 5TE sensor (calibrated in the laboratory with various type soil samples) to measure the volumetric soil moisture in the rainfed agriculture area with runoff from the private fields of Ejido "La Purisima" (Figure 2c). Additionally, three samples or measurements were collected randomly per point at 5, 10, and 20 cm depth with separations of 10 to 30 m. These activities carried out on the days that Sentinel-2 and Landsat-8 missions orbited over the studied areas.

2.3. Satellite data and image analysis

Sentinel-2 (S2) and Landsat 8 (L8) multispectral satellite images were acquired from the Google Earth Engine (GEE) platform satellite dataset catalogs (URL: https://developers.google.com/earth-engine/datasets). S2 is divided into twin satellites A and B, incorporating extensive innovations such as broadband, high spatial (10 to 60 m) and temporal resolution (10 days apart and 5 together), and 13 multispectral images spanning the visible, NIR and SWIR electromagnetic frequency domains. L8 is composed of the Operational Land Imager (OLI) and Thermal Infrared Sensor (TIRS) with 11 spectral bands in the optical and thermal infrared domain, spatial resolutions of 30 to 100 m, and temporal resolutions of 16 days.

A total of 119 Sentinel-2 and 39 Landsat-8 cloud-free images available were used to develop TOTRAM and OPTRAM pixel distributions. Moreover, 21 Sentinel-2 and 7 Landsat-8 satellite images from 2022 were analyzed for each model's calibration and validation of soil moisture (Table 2).

The flowchart of the S2 and L8 sequences of soil moisture estimation for TOTRAM and OPTRAM, and the analyzed satellite image sets are represented in Figure 3. The radiometric calibrations were performed within the GEE platform. For L8, the sets used have a radiometric calibration of their digital numbers (ND) for band 10 (10600-111900 nm) of the Top of Atmosphere (TOA) data sets at brightness temperature (BT). Furthermore, surface reflectance data sets for S2 are included in GEE; the scale factor with a value of 0.0001 was required for radiometric calibration. L8 surface reflectance data sets, two scale factors were required, 0.0000275 multiplying and 0.2

Table 2. Sampling dates and satellite images analyzed of the agricultural areas of the study.

Location	Satellite	No. images	Acquisition date (Year 2022)
Rainfed agriculture- Ejido "La Purísima" fields	Sentinel-2	6	Feb. 16, Feb.21, Feb. 26, Mar. 06, Mar. 08, Mar. 11
	Landsat-8	1	Mar.06
Surface irrigation agriculture- Chapingo Autonomous University- (URUZA) fields	Sentinel-2	11	Mar. 23, Mar. 31, Apr. 02, Apr. 05, Apr. 07, Apr. 15, Apr. 17, Jun. 14, Jun. 21, Jun. 26, Jul. 01
	Landsat-8	4	Mar. 22, Apr. 07, Jun. 10, Jun.26
Surface irrigation agriculture- Private fields near the Regional University Unit of Arid Zones (URUZA)	Sentinel-2	4	Jul. 14, Jul. 16, Jul. 24, Jul. 31
	Landsat-8	2	Jul. 12, Jul.28

subtracting the digital numbers, and 0.0001 multiplying to the emissivity band (USGS, 2022).

The reflectance of the red band [S2 band 4 (664.5 nm-A and 665 nm-B), L8 band 4 (636-673 nm)] and NIR band [(S2 band 8 (864.8 nm-A and 833nm-B), L8 band 5 (851-879 nm)] were used for the calculation of VI. The shortwave infrared band (SWIR) reflectance [S2 band 12 (2202.4 nm-A and 2185.7 nm-B), L8 band 7 (2107.4-2294 nm)] was used for STR calculation. Additionally, the Sentinel-2 SWIR band was reassembled automatically from 20 to 10 m through the red and NIR bands in GEE.

2.4. Estimation of land surface temperature (LST) using satellite imagery

Land Surface Temperature (LST) was estimated using the sensor temperature brightness (BT) in Kelvin degrees (K) (band 10) from the Landsat-8 "Top of Atmosphere (TOA)-Reflectance" satellite datasets (Chander et al., 2009) and converted to Celsius (°C). Land surface emissivity (ST_EMIS band) from the "Surface Reflectance (SR), Level 2, Collection 2, Tier 1" satellite datasets (GEE, 2022) created from the single-channel algorithm and developed by The Rochester Institute of

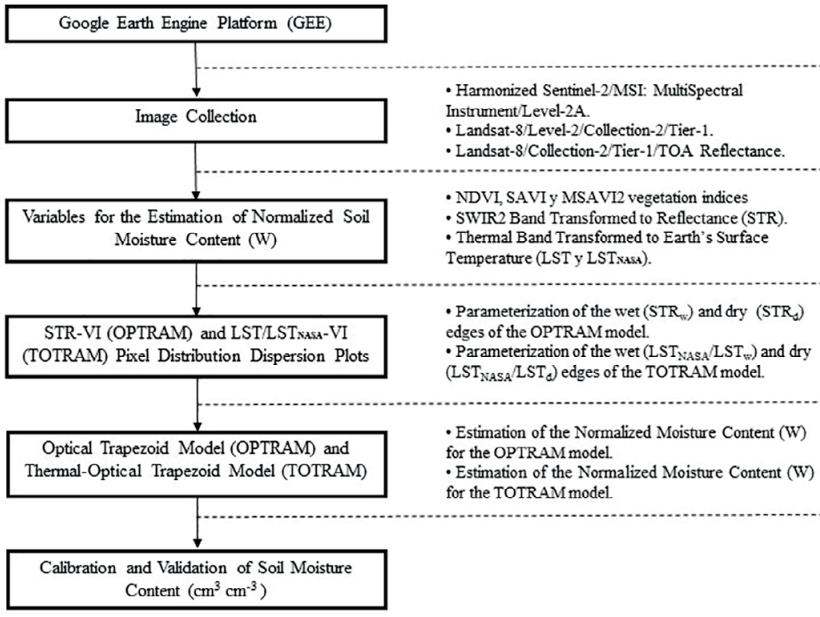

Figure 3. Flowchart illustrating the sequence of steps performed in the Sentinel-2 and Landsat-8 data analysis for soil moisture (W) estimation with OPTRAM and TOTRAM.

Technology (RIT) and The National Aeronautics and Space Administration (NASA) Jet Propulsion Laboratory (JPL) was implemented.

Consequently, combining the brightness temperature (BT) and the emissivity of the Earth's surface (Stathopoulou & Cartalis, 2007) allow estimate LST, according to Equation 1.

$$T_s = \frac{BT}{\left\{1 + \left[\left(\frac{\lambda BT}{\rho}\right)\ln\varepsilon_\lambda\right]\right\}} \quad (1)$$

Where Ts is the LST in degrees Celsius (°C), BT is the brightness temperature at the sensor, λ is the wavelength of the emitted radiation (nm should be converted to m) (Markham and Barker, 1985), ε_λ is the emissivity and ρ is defined in Equation 2.

$$\rho = h\frac{c}{\sigma} = 1.438 \times 10^{-2}\ \text{mK} \quad (2)$$

Where σ is the Boltzmann's constant (1.38×10^{-23} J/K), h is the Planck's constant (6.626×10^{-34} Js), and c is the speed of light (2.998×10^{8} m/s) (Weng et al., 2004).

In addition, an extra formula adding a thermal band (band 10) created from the single-channel algorithm and developed by The Rochester Institute of Technology (RIT) and National Aeronautics and Space Administration (NASA) Jet Propulsion Laboratory (JPL) allows the estimation of LST, following Equation 3.

$$LST_{NASA} = (ST_{B10})\times(0.00341802)+(149) \quad (3)$$

Where ST_{B10} is the thermal band (°C) of the "Surface Reflectance (SR), Level 2, Collection 2, Tier 1" satellite data sets from GEE platform catalogs.

2.5. Thermal-Optical Trapezoid Model (TOTRAM)

The Thermal-Optical Trapezoid Model, proposed by Moran et al. (1994) and Carlson et al. (1994), is based on the distribution of pixels within the LST-VI space. At present, the most commonly used vegetation index in TOTRAM model is the Normalized Difference Vegetation Index (NDVI), calculated by the difference in the amplitude of the regions of the reflectance values of the red (R) and near-infrared (NIR) spectral bands proposed by Rouse (1973), using Equation 4.

$$NDVI = \frac{\text{NIR Band} - \text{Red Band}}{\text{NIR Band} + \text{Red Band}} \quad (4)$$

In the early stages of crop growth, vegetation cover is scarce. Under these conditions, vegetation indices such as the Soil Adjusted Vegetation Index (SAVI), proposed by Huete (1988), incorporates an adjustment factor of "L" with an average value of 0.5, placed in the denominator of the NDVI equation (Equation 5).

$$SAVI = \left(\frac{\text{NIR Band} - \text{Red Band}}{\text{NIR Band} + \text{Red Band} + L}\right)(1 + L) \quad (5)$$

Whereas the Modified Soil Adjusted Vegetation Index (MSAVI2) proposed by Qi, (1994) using Equation 6, shows a better behavior than SAVI because it presents a greater sensitivity to bare soil and sparse vegetation since it takes into account the effect of soil brightness.

$$MSAVI2 = \frac{(2 + \text{NIR Band} + 1) - \sqrt{(2 + \text{NIR Band} + 1)^2 - 8(\text{NIR Band} - \text{Red Band})}}{2} \quad (6)$$

The TOTRAM model is based on the linear relationship between surface soil moisture (Θ) and LST, represented by Equation 7.

$$W = \frac{\theta - \theta_d}{\theta_w - \theta_d} = \frac{LST_d - LST}{LST_d - LST_w} \quad (7)$$

Where W is the normalized soil moisture content by the local minimum of dry soil moisture content (Θ_d) and the local minimum of wet soil moisture content (Θ_w). The terms LST_d and LST_w are the land surface temperatures in dry and wet soils, respectively. Where LST_d and LST_w are obtained by the LST-VI relationship (Figure 4) for a specific area. The upper part is considered the dry edge (Equation 8), and the lower part is considered the trapezoid's wet edge (Equation 9), which are used to solve LST_d and LST_w within the VI.

$$LST_d = i_d + s_d VI \quad (8)$$

$$LST_w = i_w + s_w VI \quad (9)$$

By combining Equations 7, 8, and 9, the soil moisture for each pixel can be estimated as a function of LST and VI, using the equation 10.

$$W = \frac{i_d + i_d VI - LST}{i_d - i_w + (s_d - s_w)VI} \quad (10)$$

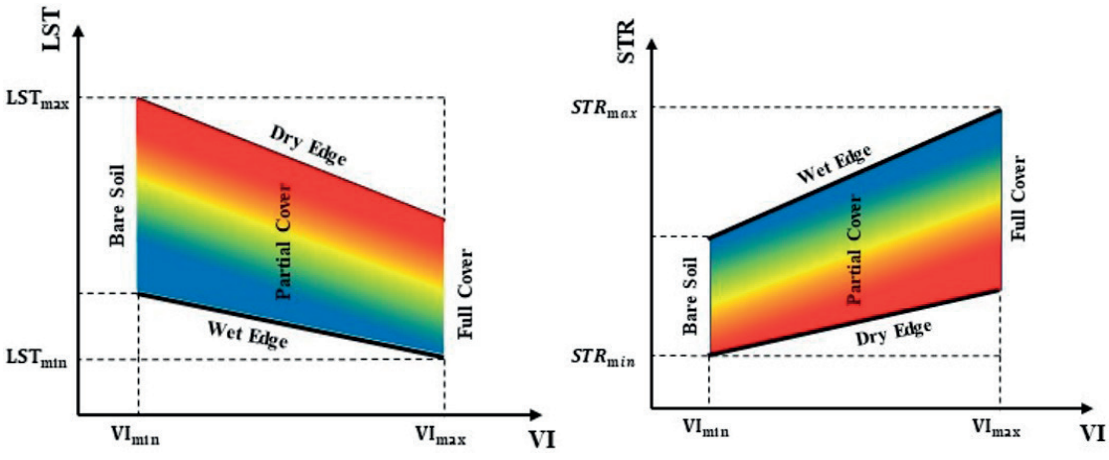

Figure 4. Parameters of the traditional termal-optical model [Eq. (10), TOTRAM] and the optical trapezoid model [Eq. (15), OPTRAM] and pixel distributions within the LST-VI and STR-VI spaces (own elaboration).

2.6. Optical Trapezoid Model (OPTRAM)

The OPTRAM model incorporate the linear relationship of STR-VI (Figure 4), developed by Sadeghi et al. (2017) as a physical model for the linear relationship between surface moisture content and the shortwave infrared (SWIR) band, transformed to reflectance (STR) (Equation 11).

$$W = \frac{\theta - \theta_d}{\theta_w - \theta_d} = \frac{STR - STR_d}{STR_w - STR_d} \quad (11)$$

In the previous equation, STR is the SWIR transformed to reflectance, STR_d and STR_w are the local minimum and maximum STR of dry (Θ_d) and wet (Θ_w) soil moisture content. The STR proposed by Sadeghi et al. (2015) is related to the SWIR reflectance (R_{SWIR}) (Equation 12).

$$STR = \frac{(1 - R_{SWIR})^2}{2R_{SWIR}} \quad (12)$$

Where STR_d and STR_w are obtained by the relationship of the STR-VI for a specific area. The upper part is considered the wet edge (Equation 13), and the lower part is considered the trapezoid's dry edge (Equation 14), which are used to solve STR_d and STR_w within the VI.

$$STR_w = i_w + s_w VI \quad (13)$$

$$STR_d = i_d + s_d VI \quad (14)$$

The combination of Equations 11, 13, and 14 is used to estimate soil moisture for each pixel as a function of STR and VI (Equation 15).

$$W = \frac{i_d + i_d VI - STR}{i_d - i_w + (s_d - s_w)VI} \quad (15)$$

3. Results

3.1. TOTRAM and OPTRAM parameterization

The TOTRAM (Equation 10) and OPTRAM (Equation 15) were parameterized based on the pixel distribution of the combination of surface irrigated and rainfed agricultural areas within the LST-VI and STR-VI spaces [LST/STR-NDVI (Figure 5), LST/STR-SAVI (Figure 6) and LST/STR-MSAVI2 (Figure 7)] respectively.

For OPTRAM in both missions (S2 and L8), the combination of pixel distributions within the STR-VI spacings are depicted in the upper part of Figures 5, 6, and 7, did not show a trapezoid-like pattern or shape. In order to acquire edge parameters and estimate soil moisture, nonlinear alternatives between the ranges of 0 to 0.9 within the VI were implemented to obtain the best equations for each pixel distribution (Table 3).

On the other hand, the LST-VI spaces in TOTRAM were parameterized by a visual inspection of the combination of the pixel distributions (Carlson, 2013), presenting a slightly trapezoid-like shape,

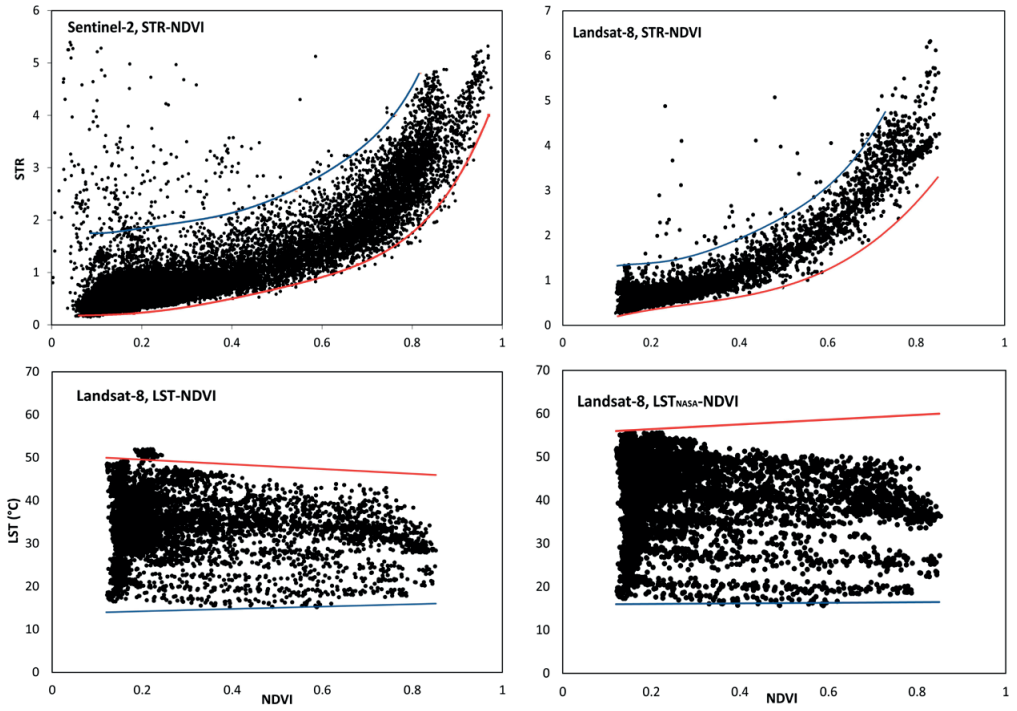

Figure 5. Pixel distributions of the combination of surface irrigated and rainfed agricultural areas within the STR-NDVI (OPTRAM) and LST-NDVI (TOTRAM) spaces; the red line represents the dry edge and the blue line the wet Edge (own elaboration).

represented in the lower part of Figures 5, 6, and 7, implementing linear edges to obtain the best distribution equations (Table 4). However, the parameterizations between the dry edges of the LST-VI and LST_{NASA}-VI distributions showed a significant difference. The dry edge in the

Table 3. Best equations obtained for the wet (STR_w) and dry (STR_d) edges for the OPTRAM model.

	Landsat-8	
	Wet edges	Dry edges
NDVI	$STR_w = -318.38NDVI^6 + 924.35NDVI^5 - 1012.4NDVI^4 + 541.32NDVI^3 - 141.59NDVI^2 + 18.16NDVI + 0.4325$	$STR_d = 11.792NDVI^3 - 10.195NDVI^2 + 4.2675NDVI - 0.1949$
SAVI	$STR_w = -2906.5SAVI^6 + 5874.1SAVI^5 - 4575.3SAVI^4 + 1760.9SAVI^3 - 342.25SAVI^2 + 33.231SAVI + 0.0648$	$STR_d = 35.754SAVI^3 - 31.486SAVI^2 + 10.381SAVI - 0.7013$
MSAVI2	$STR_w = -650.87MSAVI2^6 + 1365.1MSAVI2^5 - 1136.4MSAVI2^4 + 495.61MSAVI2^3 - 108.31MSAVI2^2 + 12.473MSAVI2 + 0.8403$	$STR_d = 11.978x^3 - 7.0858x^2 + 3.2215x - 0.1144$
	Sentinel-2	
	Wet edges	Dry edges
NDVI	$STR_w = 274.49NDVI^6 - 686.76NDVI^5 + 675.38NDVI^4 - 323.06NDVI^3 + 80.002NDVI^2 - 8.5951NDVI + 2.0712$	$STR_d = 26.568NDVI^5 - 44.046NDVI^4 + 25.083NDVI^3 - 3.3776NDVI^2 + 0.3093NDVI + 0.1686$
SAVI	$STR_w = 154.98SAVI^5 - 201.9SAVI^4 + 101.78SAVI^3 - 18.166SAVI^2 + 2.0873x + 1.61$	$STR_d = 85.568SAVI^5 - 128.83SAVI^4 + 70.095SAVI^3 - 14.705SAVI^2 + 2.0199SAVIx + 0.0293$
MSAVI2	$STR_w = 952.8MSAVI2^6 - 2026.9MSAVI2^5 + 1698.8MSAVI2^4 - 704.93MSAVI^3 + 156.02MSAVI2^2 - 15.735MSAVI2 + 2.2834$	$STR_d = 31.199MSAVI2^5 - 52.147MSAVI2^4 + 33.236MSAVI2^3 - 7.6363MSAVI2^2 + 1.6994MSAVI2 + 0.0281$

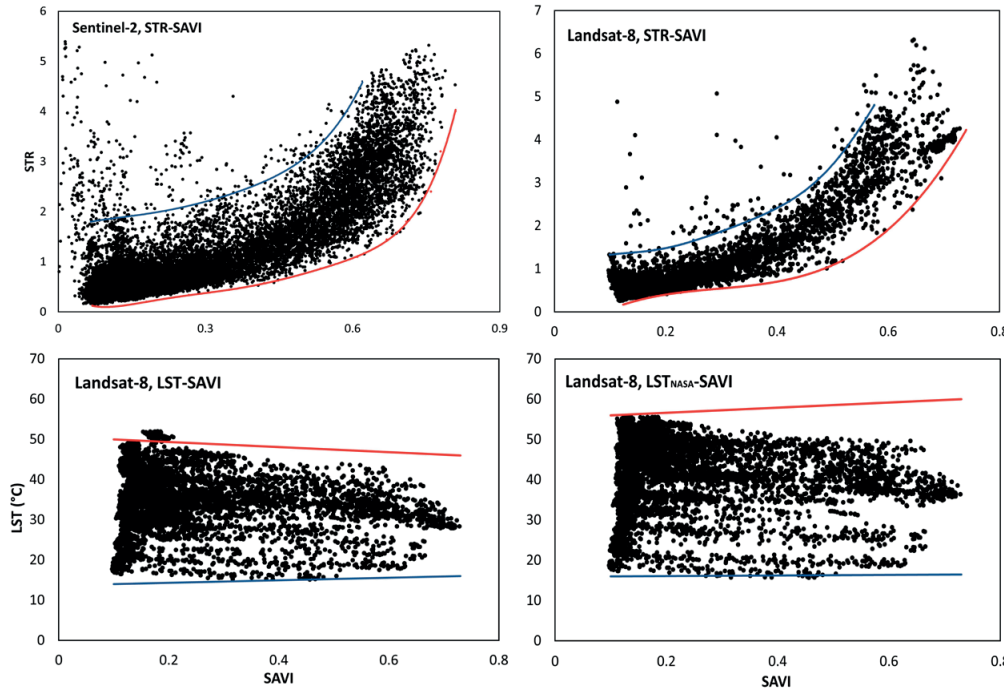

Figure 6. Pixel distributions of the combination of surface irrigated and rainfed agricultural areas within the STR-SAVI (OPTRAM) and LST-SAVI (TOTRAM) spaces; the red line represents the dry edge, and the blue line the wet edge (own elaboration).

LST_{NASA}-VI distributions presents an increase in the slope of the end part of the dry edge for ranges from 0.1 to 0.9 within the VI, as opposed to the LST-VI distributions, where the end part of the dry edge presents a very slight decrease in the slope at the end part.

3.2. Volumetric soil moisture estimations

The results indicate that calibrations of both models and validations of measured volumetric soil moisture data (Θ) compared with estimated data (W) at different depths of OPTRAM and TOTRAM using NDVI (Figure 8), obtained at 10 cm of depth the most accurate linear relationships for OPTRAM in both missions (S2 and L8) with RMSE of 0.035 and 0.0444 $cm^3\ cm^{-3}$; R^2 of 0.7107 and 0.7696, respectively. In TOTRAM, the LST-NDVI and LST_{NASA}-NDVI relationships showed the most accurate results at 20 cm and 10 cm depth with RMSE of 0.0485 and 0.0484 $cm^3\ cm^{-3}$; R^2 of 0.8404 and 0.7203, respectively.

Table 4. Best equations obtained for the wet (LST_{NASA}/LST_w) and dry (LST_{NASA}/LST_d) edges for the TOTRAM model.

Landsat-8		
LST	Wet edges	Dry edges
NDVI	LST_w = 2.7322NDVI + 13.672	LST_d = -5.4645NDVI + 50.656
SAVI	LST_w = 3.1746SAVI + 13.683	LST_d = -6.3492SAVI+ 50.635
MSAVI2	LST_w = 2.9412MSAVI2 + 13.706	LST_d = -5.8824MSAVI2 + 50.588
LST_{NASA}		
NDVI	LST_{NASAw} = 0.6849NDVI+ 15.918	LST_{NASAd} = 5.4795NDVI + 55.342
SAVI	LST_{NASAw} = 0.7937SAVI+ 15.921	LST_{NASAd} = 6.3492SAVI + 55.365
MSAVI2	LST_{NASAw} = 0.7353MSAVI2 + 15.926	LST_{NASAw} = 5.8824MSAVI2 + 55.412

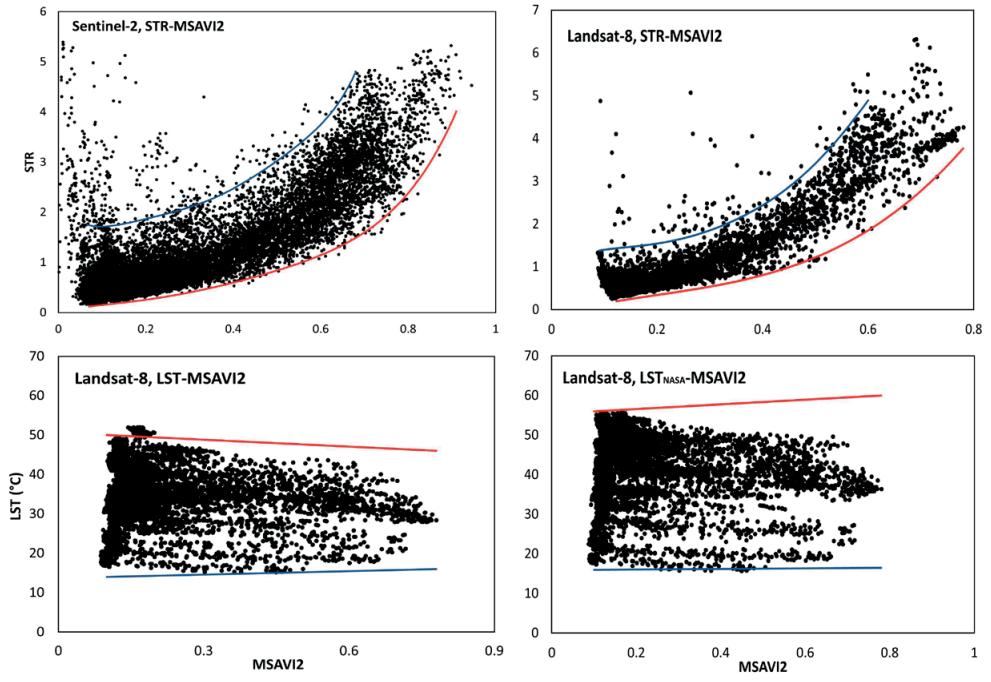

Figure 7. Pixel distributions of the combination of surface irrigated and rainfed agricultural areas within the STR-MSAVI2 (OPTRAM) and LST-MSAVI2 (TOTRAM) spaces; the red line represents the dry edge, and the blue line the wet edge (own elaboration).

Moreover, SAVI with OPTRAM (Figure 9) showed the most accurate linear relationships at 20 cm and 5 cm depth (S2 and L8) with RMSE of 0.0362 and 0.0359 cm^3 cm^{-3} and R^2 of 0.7469 and 0.8045, respectively. TOTRAM the most accurate linear relationships (LST and LST_{NASA}) were obtained at 10 cm and 5 cm depth with RMSE of 0.0461 and 0.0513 cm^3 cm^{-3}; R^2 of 0.8488 and 0.7581, respectively.

Additionally, MSAVI2 with OPTRAM (Figure 10) comparisons showed the most accurate linear relationships at 20 cm depth for both missions (S2 and L8) with RMSE of 0.0339 and 0.428 cm^3 cm^{-3}; R^2 of 0.6973 and 0.7647, respectively. In contrast to TOTRAM, the most accurate linear relationships at 10 cm depth for both relationships (LST and LST_{NASA}) with RMSE of 0.0467 and 0.045 cm^3 cm^{-3}; R^2 of 0.8511 and 0.7457, respectively.

3.3. Soil moisture maps

The W maps were generated from the dates S2 and L8 share the same satellite image acquisition day for each pixel distribution within OPTRAM and TOTRAM. The first date (Figure 11) of the Ejido "La Purisima" area comprises bare soil for all VI with ranges between 0.1 to 0.25. The OPTRAM model showed overestimations in W with values between 0.3 to 0.55 cm^3 cm^{-3}, even overestimating twice the measured data (Θ) at 20 cm depth for all distributions of both missions. The reason may lie in the combination of the pixel distributions of the agricultural types since both areas of surface irrigated agriculture have a larger irrigated area, observing more data from STR-VI relationships than those of rainfed agriculture and the dry/wet edges chosen. In addition, it was observed that at high STR (0.8-1) and low VI (0.1-0.25), soil moisture is more likely to be overestimated by the established edges. Because of this W obtained from the Ejido

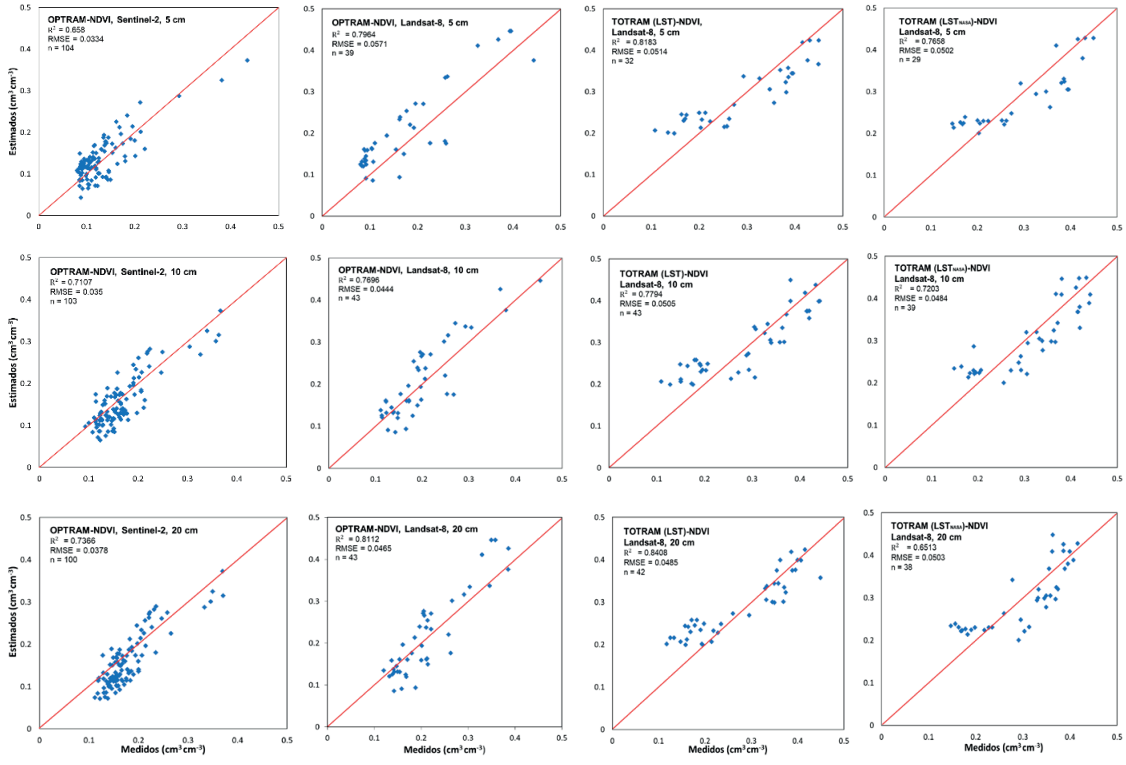

Figure 8. OPTRAM and TOTRAM soil moisture estimates using NDVI compared to in situ measured data from surface irrigated and rainfed agricultural areas (own elaboration).

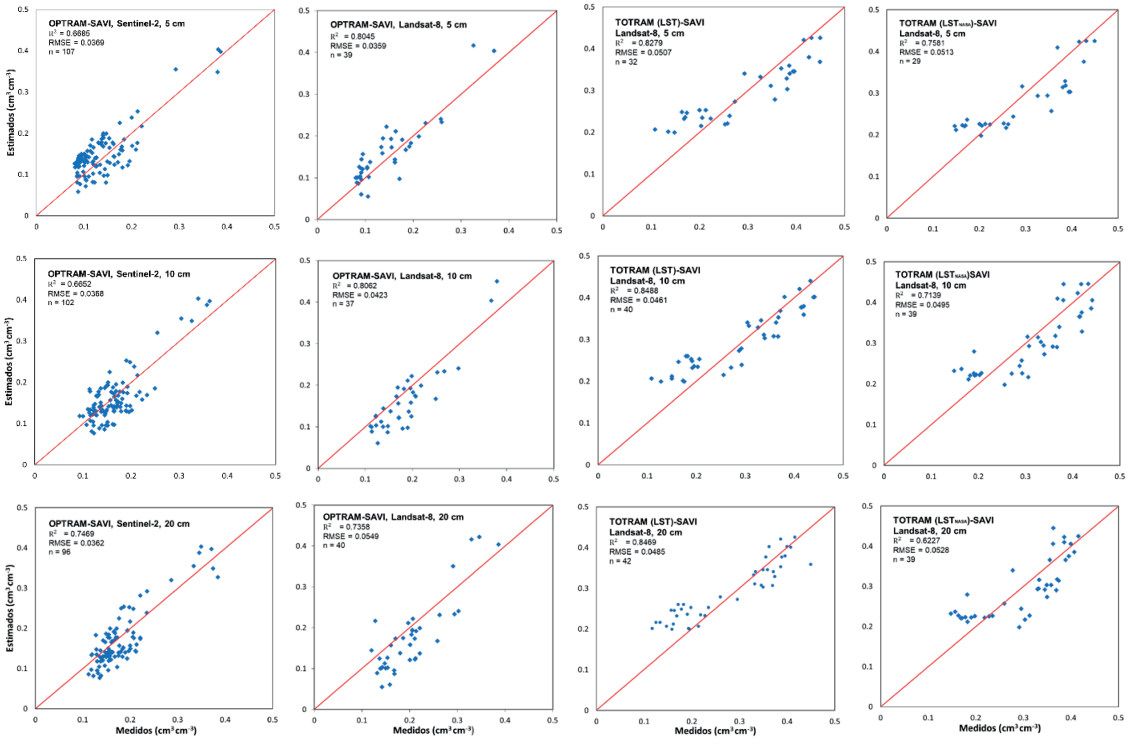

Figure 9. OPTRAM and TOTRAM soil moisture estimates using SAVI compared to in situ measured data from surface irrigated and rainfed agricultural areas (own elaboration).

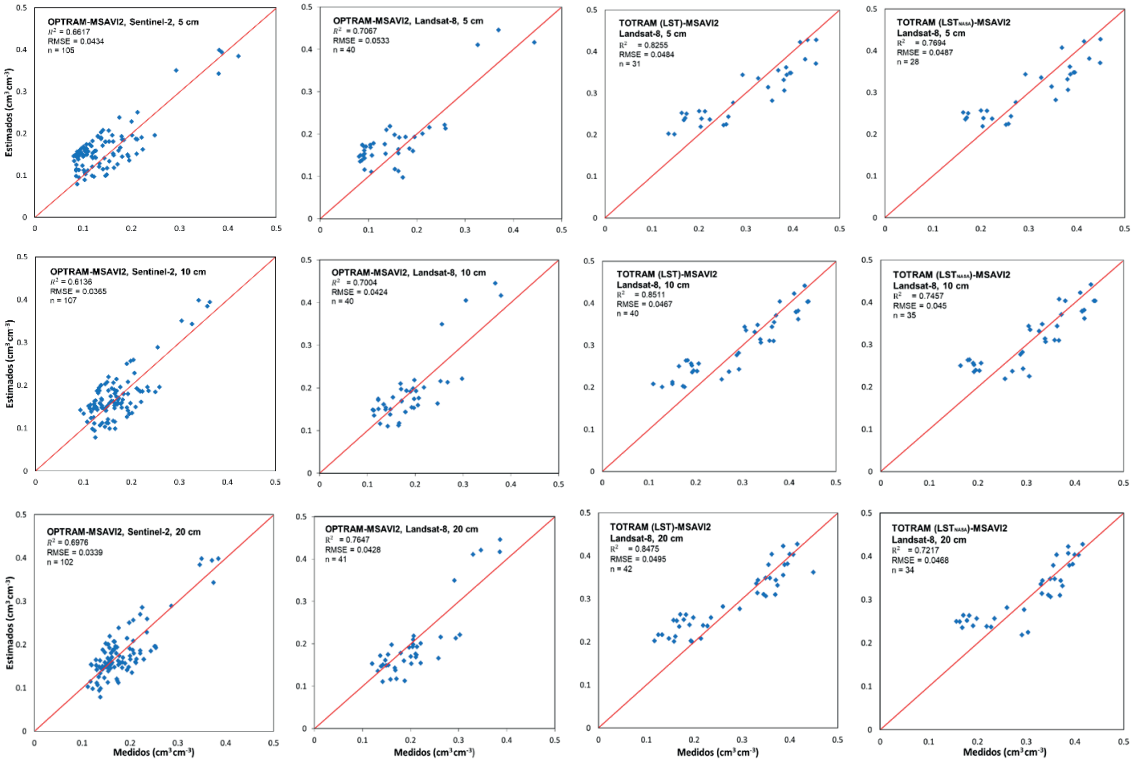

Figure 10. OPTRAM and TOTRAM soil moisture estimates using MSAVI2 compared to in situ measured data from surface irrigated and rainfed agricultural areas (own elaboration).

"La Purísima" area with rainfed agriculture was not considered for the validation due to the overestimates presented.

Likewise, TOTRAM for the LST_{NASA}-VI relationship showed the same behavior as OPTRAM, the overestimation is presented when the VI (0.1-0.25) and the LST_{NASA} temperatures (<46°C) are low, possibly caused by the parameterization of its dry edge. Besides, It should be emphasized that LST_{NASA} reveals an increase of around 7-8°C over LST in each pixel. On the other hand, the LST-VI relationships did not present overestimations. Instead, they showed correct behavior throughout the calibration within the different depths due to the parameterizations of their edges.

On the second date, the gravity irrigation area of the Chapingo Autonomous University-URUZA (Figure 12) presents VI ranges between 0.1 to 0.45. The W maps in OPTRAM show a substantial similarity of W estimates for both missions with ranges between 0.1 to 0.3 cm^3 cm^{-3} and presenting significantly accurate VI-W relationships with STR levels between 0.4 to 0.6 and VI between 0.1 to 0.45. In addition, it was observed that OPTRAM, employing Landsat-8 observations, estimates more accurately the moisture of bare soils with conventional type tillage after their respective irrigations, observed in the third parcel (Figure12; sections c, h, and m) and occurs when VI is less than 0.15 and STR is higher than 0.48. In the other hand, TOTRAM in LST-VI and LST_{NASA}-VI relationships presented overestimations and homogeneity of W with values between 0.35 to 0.45 cm^3 cm^{-3}, overestimating the measured data (Θ) at 20 cm depth, caused by low temperatures for both relationships. Low temperatures are considered for LST less than 38 °C and LST_{NASA} less than 46 °C for the established wet and dry edge parameters. If land surface temperatures and VI present low levels, soil moisture is more likely to be overestimated.

The third date (Figure 13), located in the same area as the second date, presented VI ranges

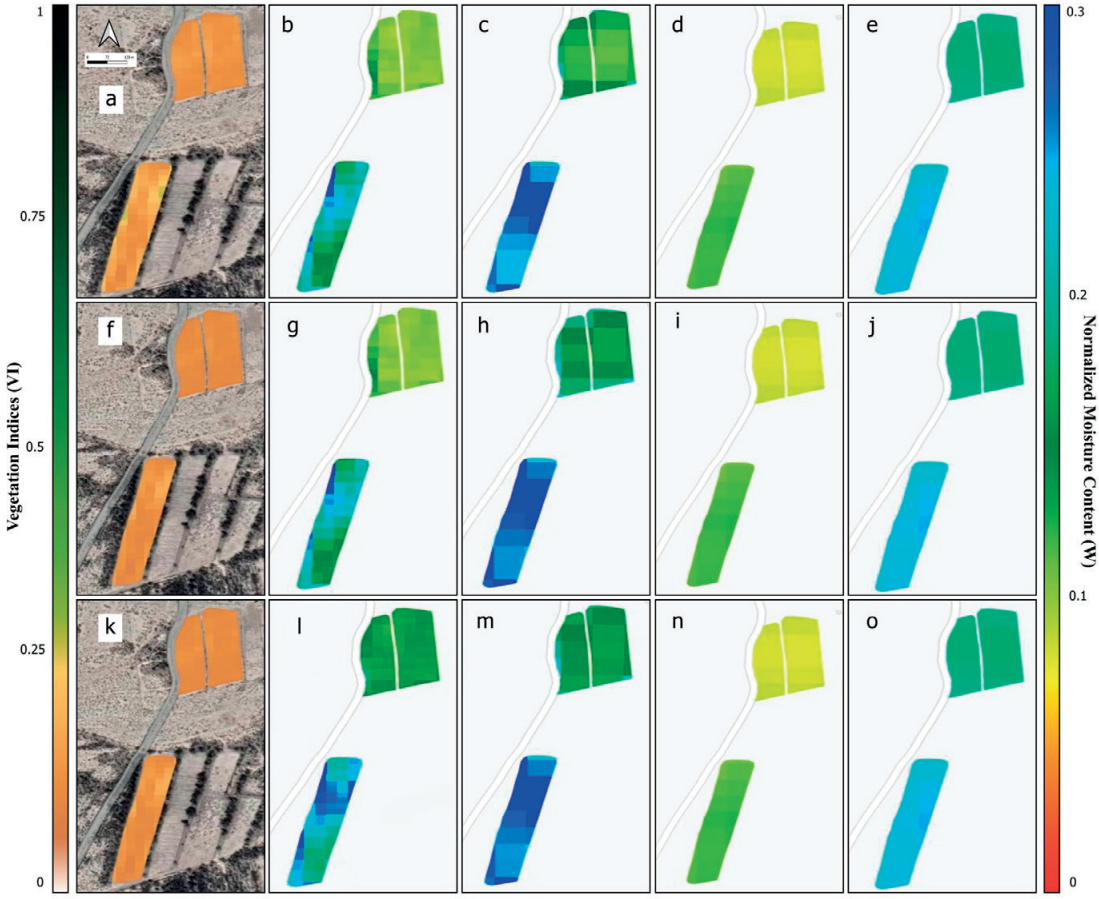

Figure 11. Location Ejido "La Purisima" Durango, Mexico; (a, f, k) NDVI, SAVI, and MSAVI2 obtained with Sentinel-2, respectively (date: March 06, 2022): (b, c) NDVI, (g, h) SAVI and (l, m) MSAVI2, W in OPTRAM for Sentinel-2 and Landsat-8, respectively. TOTRAM model, (d, e) NDVI, (i, j) SAVI, and (n, o) MSAVI2 for LST-VI and LST_{NASA}-VI relationships, respectively (own elaboration).

between 0.1 to 0.75. The OPTRAM model, through Landsat-8, presented overestimations in W within VI ranges between 0.4 to 0.75 (second and third parcels, sections c, h y m), possibly caused by the high STR levels (higher than 1.6) and the parameterizations of the dry edge. On the other hand, Sentinel-2 did not show homogeneity in W but precise ranges between 0.1 to 0.35 cm^3 cm^{-3} within the same ranges of VI and fields as Landsat-8. The TOTRAM relationships showed homogeneity in W, with precise VI-W relations between 0.15 to 0.35 cm^3 cm^{-3}, presenting LST_{NASA} and LST temperatures on bare soil (0.1-0.25) between 52 °C and 44 °C, and with dense vegetation (0.5-0.75) between 44 °C and 36 °C, respectively.

4. Discussion

Studies for soil moisture estimation at different depths with bare, semi-bare, and vegetation-covered soil have been developed in the near-past. Hassanpour et al. (2020) compare OPTRAM at two depths (surface and root moisture) through linear and nonlinear edge parameterization using three different pixel distributions (bare soil, vegetated soil and combined). In that case, the highest R^2 was 0.803, and the lowest RMSE was 0.030 cm^3 cm^{-3}, obtained on surface soil moisture using nonlinear edges from the bare soil pixel distributions. However, the combination of the distribution of soils with vegetation cover and bare soils obtained a slightly lower result in R^2

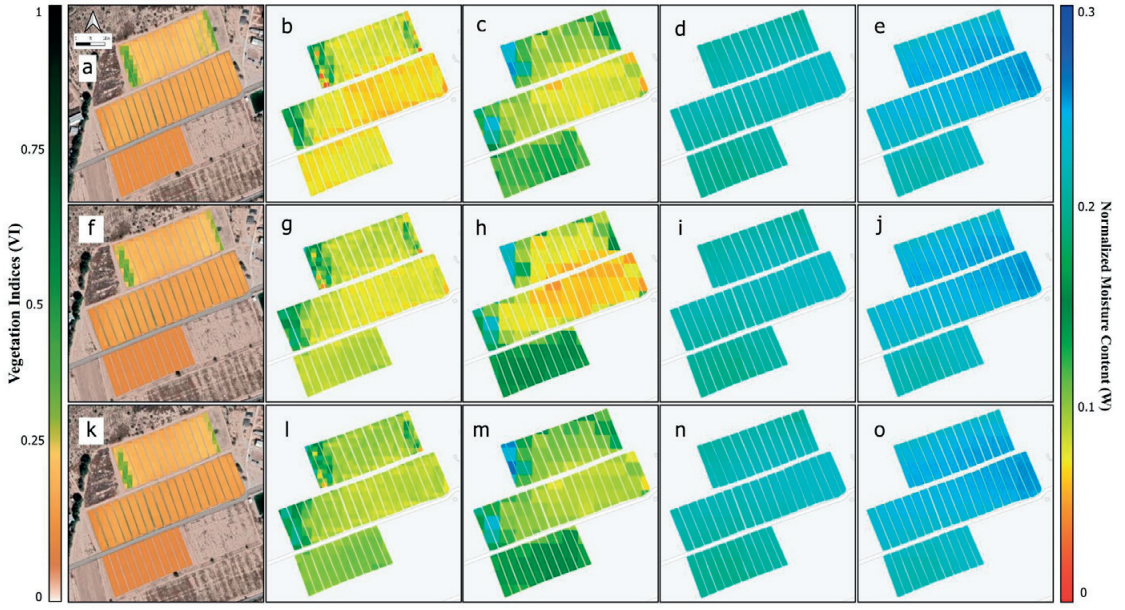

Figure 12. Location Chapingo Autonomous University- Regional University Unit of Arid Zones (URUZA**)** Durango, Mexico; (a, f, k) NDVI, SAVI, and MSAVI2 obtained with Sentinel-2, respectively (date: April 07, 2022): (b, c) NDVI, (g, h) SAVI and (l, m) MSAVI2, W in OPTRAM for Sentinel-2 and Landsat-8, respectively. TOTRAM model, (d, e) NDVI, (i, j) SAVI, and (n, o) MSAVI2 for LST-VI and LST_{NASA}-VI relationships, respectively (own elaboration).

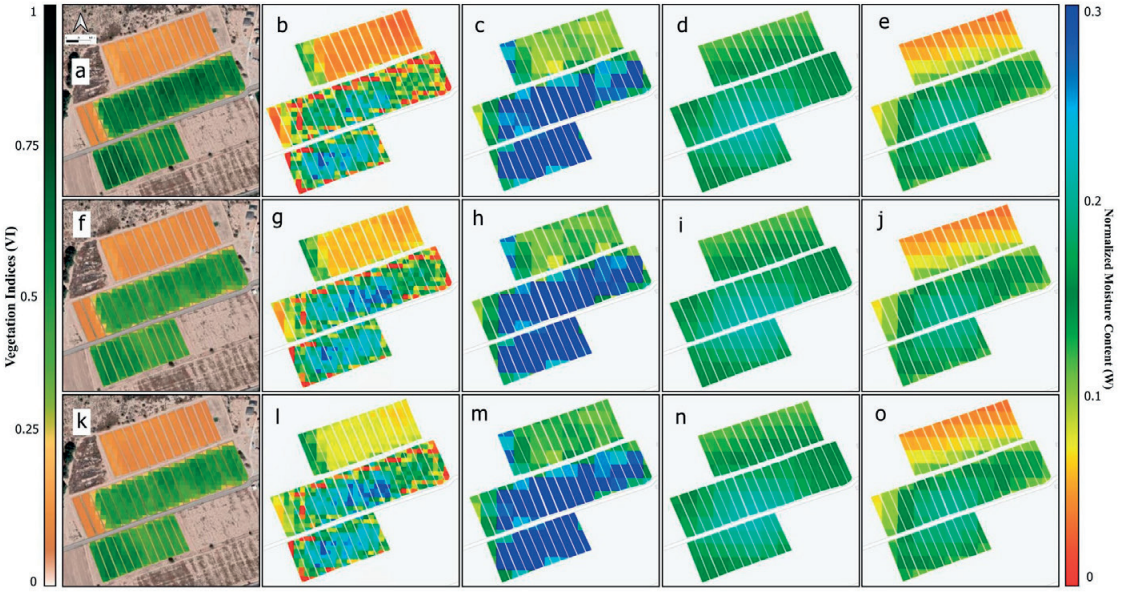

Figure 13. Location Chapingo Autonomous University- Regional University Unit of Arid Zones (URUZA**)** Durango, Mexico; (a, f, k) NDVI, SAVI, and MSAVI2 obtained with Sentinel-2, respectively (date: June 26, 2022): (b, c) NDVI, (g, h) SAVI and (l, m) MSAVI2, W in OPTRAM for Sentinel-2 and Landsat-8, respectively. TOTRAM model, (d, e) NDVI, (i, j) SAVI, and (n, o) MSAVI2 for LST-VI and LST_{NASA}-VI relationships, respectively (own elaboration).

of 0.75 and higher in RMSE of 0.036 cm^3 cm^{-3}. The parameterized edges and dates chosen for developing the pixel distributions showed good accuracy for estimating surface soil moisture between 0 and 5 cm depth. The Optical Trapezoid Model (OPTRAM) can be parametrized universally. Babaeian et al. (2018) evaluate how the parametrization of OPTRAM works for long periods of time (several decades). Especially relevant for soil moisture and agricultural drought in response to climate change implementing analysis of MODIS satellite observations from 2001 to 2017.The OPTRAM soil moisture estimates were compared with missions as the Soil Moisture Active and Pasive (SMAP), the Soil Moisture Ocean Salinity (SMOS) and the Advance Scatterometer (ASCAT). The performance of OPTRAM is comparable with the ASCAT, but slightly less accurate than SMAP and SMOS. Evaluation results indicate RMSE and R between 0.050 and 0.085 cm^3 cm^{-3} and 0.1 to 0.70, respectively.

Besides, studies have parameterized edges nonlinearly for soil moisture estimation in TOTRAM; Mallick et al. (2009) estimated the volumetric surface moisture (Θ) in cultivated soils from selected agricultural regions in India. Nonlinear trends in dry edge at high NDVI ranges and a sloping wet edge were found. However, the hypothesized linear dry and horizontal wet edge combination provided better results. On the other hand, Sadeghi (2017) compared the performance between OPTRAM and TOTRAM in two watersheds in Arizona and Oklahoma, United States of America, revealing that the RMSE of TOTRAM are slightly better for daily comparisons than those of OPTRAM in most cases. As a matter of fact, TOTRAM was able to capture the temporal variation of mean soil moisture across watersheds but failed to capture the detailed spatial variability of soil moisture and stating the strong relationship between volumetric soil moisture (Θ). Highlighting the temporal dependence due to changes in ambient atmospheric parameters and concluding the feasibility of a universal calibration for OPTRAM but not for TOTRAM.

The two-year time series combination analysis of pixel distributions for OPTRAM and TOTRAM at different depths of the study presented accurate soil moisture estimates for bare soils and the presence of vegetation cover. The difference between the models is centered on the VI, STR, and LST ranges. As shown in Figures (11, 12, and 13), OPTRAM is susceptible to different ranges between STR and VI, showing overestimates due to increasing STR (>0.8) and low VI (<0.20) levels and high STR (>1.6) with high VI (>0.5) levels. Whereas TOTRAM is susceptible to low levels of LST in bare soils as shown in Figure 12, overestimating soil moisture in low levels of LST and VI. There are significant differences between OPTRAM and TOTRAM for soil moisture estimation, but OPTRAM was more accurate for soils with VI ranges less than 0.5 than TOTRAM, and TOTRAM was more accurate for VI ranges greater than 0.5. In this case, possible reasons that affected could lie in time series distributions, edge parameterizations, exposure of soil moisture to solar radiation, furrow spacing, vegetation ratio, and crop dates.

5. Conclusions

This study observed the uses of each model for soil moisture estimation in partially dry bare soils, wet bare soils using surface irrigation with conventional tillage, and soils covered by dense vegetation. The OPTRAM model obtained the most accurate linear relationships (W-Θ) using SAVI at 20 cm with Sentinel-2 and 5 cm with Landsat-8, estimating soil moisture more accurately in partially dry and wet bare soils using conventional tillage irrigation for soil management. In comparison, TOTRAM using Landsat-8, obtained the most accurate linear relationship at 10 cm depth by LST-VI relationship implementing MSAVI2, estimating soil moisture more accurately with higher vegetation cover. As a result, SAVI and MSAVI2 obtained the best results because the locations presented slightly wider spacing between furrows than average, resulting in a greater presence of the effect of ground gloss. However, the pixel distributions and edges selected for OPTRAM soil estimation were not feasible for any depth and vegetation index within rainfed agriculture with runoff. In contrast, TOTRAM correctly estimated soil moisture for surface irrigation and rainfed agriculture with runoff at different depths. The models can be used for different vegetative

stages and VI levels. Initially, OPTRAM showed higher accuracy at lower ranges and TOTRAM at higher crop VI ranges. In sum, due to the spatial variability and atmospheric changes of the environment at different times of the year. An alternative for improving soil moisture estimation by implementing time series could be the separation of the vegetative stages of the crops. The separation between the vegetative stage would provide completely different edges and ranges without incorporating STR, LST, and VI that has not been present in the chosen growth stage to avoid overestimating soil moisture when STR increases or LST decreases.

Acknowledgements

This research was supported by the Consejo Nacional de Ciencia y Tecnología (CONACYT), Universidad Autónoma Chapingo, and INIFAP-CENID RASPA Centro Nacional de Investigación Disciplinaria en Relación Agua-Suelo-Planta-Atmósfera.

References

Ambrosone, M., Matese, A., Di Gennaro, S.F., Gioli, B., Tudoroiu, M., Genesio, L., & Toscano, P. 2020. Retrieving soil moisture in rainfed and irrigated fields using Sentinel-2 observations and a modified OPTRAM approach. *International Journal of Applied Earth Observation and Geoinformation*, *89*, 102113. https://doi.org/10.1016/j.jag.2020.102113

Babaeian, E., Sadeghi, M., Franz, T.E., Jones, S., & Tuller, M. 2018. Mapping soil moisture with the OPtical TRApezoid Model (OPTRAM) based on long-term MODIS observations. *Remote sensing of environment*, *211*, 425-440. https://doi.org/10.1016/j.rse.2018.04.029

Bouyoucos, G.J. 1936. Directions for making mechanical analyses of soils by the hydrometer method. *Soil Science*, *42*(3), 225-230. https://doi.org/10.1097/00010694-193609000-00007

Carballo, H.R., & Sandoval, A.P. 2007. Evaluación participativa de la degradación del suelo en la Reserva de la Biosfera de Mapimi, Durango, México. *Revista Chapingo Serie Zonas Aridas*, *6*(2), 247-254.

Carlson, T.N., Gillies, R.R., & Perry, E.M. 1994. A method to make use of termal infrared temperatura and NDVI measurements to infer surface soil water content and fractional vegetation cover. *Remote Sensing Reviews, 9*(1-2), 161-173. https://doi:10.1080/02757259409532220

Carlson, T.N. 2013. Triangle models and misconceptions. *International Journal of Remote Sensing Applications*, *3*(3), 155-158.

Chander, G., & Helder, D.L. 2009. Summary of current radiometric calibration corfficients for Landsat MSS, TM, ETM+, and EO-1 ALI sensors. *Remote Sensing and Environment*, *113*(5), 893-903. https://doi.org/10.1016/j.rse.2009.01.007

Dane, J.H., & Topp, G.C. 2002. Thermogravimetric determinations using convective oven-drying. In: Dane and G.C. Topp (eds). *Methods of soil analysis. Part 4. physical methods*. Soil Society of America, Inc., Madison. https://doi.org/10.2136/sssabookser5.4

Davis, J.L., & Chudoviak, W.J. 1975. In situ meter for measuring relative permitive of soil. *Geological Survey of Canada*. Paper no. 75-1A, 1975 p. 75-79, https://doi.org/10.4095/104349

Dobriyal, P., Qureshi, A., Badola, R., & Hussain, S.A. 2012. A review of the methods available for estimating soil moisture and its implications for water resource management. *Journal of Hydrology*, *458*, 110-117. https://doi.org/10.1016/j.jhydrol.2012.06.021

García, G.I., & Martínez, J.G. 2004. Caracterización de la Reserva de la Biosfera Mapimí Mediante el uso de sistemas de información geográfica. In *Memorias del IV Simposio Internacional sobre la Flora Silvestre en Zonas Áridas*. Universidad Autónoma de Chihuahua-Universidad de Sonora.

Google Earth Engine. *Landsat Algorithms, Landsat collection structure.* Retrived January 15, 2022, from https://developers.google.com/earth-engine/guides/landsat.

Hassanpour, R., Zarehaghi, D., Neyshabouri, M.R., Feizizadeh, B., Rahmati M. 2020. Modification on optical trapezoid model for accurate estimation of soil moisture content in a maize growing field. *Journal of Applied Remote Sensing, 14*(3), 034519-034519. https://doi.org/10.1117/1.JRS.14.034519

Huete, A.R. 1988. A soil-adjusted vegetation index (SAVI). *Remote sensing of environment, 25*(3), 295-309. https://doi:10.1016/0034-4257(88)90106-x

Lakhankar, T., Krakauer, N., & Khanbilvardi, R. 2009. Applications of microwave remote sensing of soil moisture for agricultural applications. *International Journal of Terraspace Science and Engineering*, *2*(1), 81-91. https://doi.org/10.3390/rs1020080

Lakshmi, V. 2012. Remote sensing of soil moisture. International *Scholarly Research Notices Soil Sciences,* 2013, 1-33. https://doi.org/10.1155/2013/424178

Mallick, K., Bhattacharya, B.K., & Patel, N.K. 2009. Estimating volumetric surface moisture content for cropped soils using a soil wetness index based on surface temperature and NDVI. *Agricultural and Forest Meteorology*, *149*(8), 1327-1342. https://doi:10.1016/j.agrformet.2009.03.004

Mananze, S., Pôças, I., & Cunha, M. 2019. Agricultural drought monitoring based on soil moisture derived from the optical trapezoid model in Mozambique. *Journal of Applied Remote Sensing*, *13*(2), 024519-024519. https://doi.org/10.1117/1.JRS.13.024519

Markhan, B.L., & Barker, J.L. 1985. Spectral characterization of the LANDSAT Thematic Mapper sensors. *International Journal of Remote Sensing*, *6*(5), 697-716. https://doi.org/10.1080/01431168508948492

Montaña, C. 1988. Estudio integrado de los recursos vegetación, suelo y agua en la Reserva de la Biosfera de Mapimí. *Instituto de Ecología, AC,* México, DF.

Moran, M.S., Clarke, T.R., Inoue, Y., & Vidal, A. 1994. Estimating crop water deficit using the relation between surface-air temperature and spectral vegetation index. *Remote Sensing of Environment*, *49*(3), 246-263. https://doi:10.1016/0034-4257(94)90020-5

Pandey, R., Goswami, S., Sarup, J., & Matin, S. 2021. The thermal–optical trapezoid model-based soil moisture estimation using Landsat-8 data. *Modeling Earth Systems and Environment*, *7*, 1029-1037. https://doi.org/10.1007/s40808-020-00975-8

Qi, J., Chehbouni, A., Huete, A.R., Kerr, Y.H., & Sorooshian, S. 1994. A modified soil adjusted vegetation index. *Remote Sensing of Environment*, *48*(2), 119-126. https://doi.org/10.1016/0034-4257(94)90134-1

Rahimzadeh-Bajgiran, P., Berg, A.A., Champagne, C., & Omasa, K. 2013. Estimation of soil moisture using optical/thermal infrared remote sensing in the Canadian Prairies. *ISPRS Journal of Photogrammetry and Remote Sensing*, *83*, 94-103. https://doi.org/10.1016/j.isprsjprs.2013.06.004

Rahmati, M., Weihermüller, L., Vanderborght, J., Pachepsky, Y.A., Mao, L., Sadeghi, S.H., & Vereecken, H. 2018. Development and analysis of the Soil Water Infiltration Global database. *Earth System Science Data*, *10*(3), 1237-1263. https://doi.org/10.5194/essd-10-1237-2018

Rouse, J.W. 1973. Monitoring the vernal advancement and retrogradation of natural vegetation [NASA/GSFCT Type II Report]. Greenbelt, MD: NASA/Goddard Space Flight Center.

Sadeghi, M., Jones, S.B., & Philpot, W.D. 2015. A linear physically-based model for remote sensing of soil moisture using short wave infrared bands. *Remote Sensing of Environment*, *164*, 66-76. https://doi.org/10.1016/j.rse.2015.04.007

Sadeghi, M., Babaeian, E., Tuller, M., & Jones, S.B. 2017. The optical trapezoid model: A novel approach to remote sensing of soil moisture applied to Sentinel-2 and Landsat-8 observations. *Remote sensing of environment*, *198*, 52-68. https://doi.org/10.1016/j.rse.2017.05.041

Santos, W.J.R., Silva, B.M., Oliveira, G.C., Volpato, M.M.L., Lima, J.M., Curi, N., Marques, J.J. 2014. Soil moisture in the root zone and its relation to plant vigor assessed by remote sensing at management scale. *Geoderma, 221*, 91-95. https://doi.org/10.1016/j.geoderma.2014.01.006

Şekertekin, A., Marangoz, A.M., & Abdikan, S. 2018. Soil moisture mapping using Sentinel-1A synthetic aperture radar data. *International Journal of Environment and Geoinformatics*, *5*(2), 178-188. https://doi.org/10.30897/ijegeo.425606

Stathopoulou, M., Cartalis, C. 2007. Daytime urban heat islands From Landsat ETM+ and Corine land cover data: An application to major cities in Greece. *Solar Energy*, *81*(3), 358-368. https://doi.org/10.1016/j.solener.2006.06.014

Tabatabaeenejad, A., Burgin, M., Duan, X., & Moghaddam, M. 2014. P-band radar retrieval of subsurface soil moisture profile as a second-order polynomial: First AirMOSS results. *IEEE Transactions on Geoscience and Remote Sensing*, *53*(2), 645-658. https://doi.org/10.1109/TGRS.2014.2326839

Tollenaar, M., & Lee, E.A. 2002. Yield potential, yield stability and stress tolerance in maize. *Field crops research*, *75*(2-3), 161-169. https://doi.org/10.1016/S0378-4290(02)00024-2

United State Deparment of Agriculture. (1977). Texture Triangule USDA. *36*(1).

United States Geological Survey. 2022. *Landsat 8-9 Collection 2 (C2) Level 2 Science Product (L2SP) Guide*. Sioux Falls, South Dakota. Department of the Interior U.S. Geological Survey.

Vereecken, H., Huisman, J.A., Bogena, H., Vanderborght, J., Vrugt, J.A., & Hopmans, J.W. 2008. On the value of soil moisture measurements in vadose zone hydrology: A review. *Water resources research*, *44*(4). https://doi.org/10.1029/2008WR006829

Wang, L., & Qu, J.J. 2009. Satellite remote sensing applications for surface soil moisture monitoring: A review. *Frontiers of Earth Science in China*, *3*(2), 237-247.https://doi.org/10.1007/s11707-009-0023-7

Weng, Q., Lu, D., & Schubring, J. 2004. Estimation of land Surface temperatura-vegetation abundance relationship for urban heat islands. *Remote Sensing of Environment*, *89*(4), 467-483. https://doi:10.1016/j.rse.2003.11.005